

Supporting Information

Regular Arrays of C₆₀-Based Molecular Rotors Mounted on a Surface of Tris(*o*-phenylenedioxy)cyclotriphosphazene Nanocrystals

Carina Santos Hurtado,^a Guillaume Bastien,^a Igor Rončević,^b Martin Dračinský,^a
Teddy Tortorici,^c Charles T. Rogers,^c Josef Michl,^{a,d} and Jiří Kaleta^{a,*}

^a *Institute of Organic Chemistry and Biochemistry of the Czech Academy of Sciences, Flemingovo nám. 2, 160 00 Prague 6, Czech Republic.*

^b *Department of Chemistry, University of Oxford, Chemistry Research Laboratory, OX1 3TA Oxford, UK.*

^c *Department of Physics, University of Colorado, Boulder, Colorado 80309, United States.*

^d *Department of Chemistry and Biochemistry, University of Colorado, Boulder, Colorado 80309, United States.*

Table of Contents

Experimental part	S2
Synthesis of compounds 1 and 4	S4
Calculations of the dipole moment of molecular rotor 1	S5
Interpretation of NMR spectra	S6
Computational investigation of 1 @TPP	S9–S10
<i>Copies of NMR spectra</i>	<i>S11–S17</i>
Compound 1	S11
Compound 4	S8
References	S18

EXPERIMENTAL PART

Materials. All reactions were carried out under argon atmosphere with dry solvents freshly distilled under anhydrous conditions. The yields refer to isolated, chromatographically and spectroscopically homogeneous materials.

Compound **3** was prepared according to an already published procedure.¹ All the other reagents were used as supplied unless otherwise stated.

Transmission Electron Microscopy. The sample was prepared by dropping an aqueous suspension of 10% **1**@TPP-*d*₁₂ onto a carbon-coated copper grid and drying it in air. The images were recorded with a JEOL JEM-1011 transmission electron microscope operated at 60 kV.

X-ray Powder Diffraction. The X-ray powder patterns were taken with a Rigaku MiniFlex 600 powder X-ray diffractometer system with Cu K α radiation at the average wavelength of $\lambda = 0.15418$ nm. Powder samples, loaded into borosilicate glass capillaries of 1.0 mm in diameter and with a wall thickness of 10 μ m, were mounted on a Huber four-circle goniometer. The scattered X-rays were measured with a NaI scintillator point detector that was moved in a horizontal plane by an angle of 2θ with respect to the direction of the incident X-rays to scan the Bragg scattering profile. The resolution of the instrument, in its usual configuration, is $q_{\text{res}} \approx 0.003 \text{ \AA}^{-1}$.

Solid-State NMR. High-resolution ³¹P and ¹³C solid-state NMR spectra were obtained using a JEOL ECZ600R spectrometer operating at 243.0 MHz for ³¹P, 150.9 MHz for ¹³C, and 600.2 MHz for ¹H. The samples were packed into 3.2 mm magic-angle spinning rotors (MAS) and the measurements were taken at the MAS rates of 18 kHz. Phosphorus, carbon and nitrogen spectra were measured using cross polarization (CP); the phosphorus spectra were also measured using the single-pulse experiment. The ¹³C chemical shifts were referenced to crystalline DSS as a secondary reference ($\delta = 0.0$ ppm for CH₃ carbon). The phosphorus spectra were referenced against (NH₄)₂HPO₄ ($\delta = 1.37$ ppm). A ramped-amplitude shaped pulse was used during cross-polarization. The contact time for CP was 5 ms for ¹³C and ³¹P. The relaxation delays were estimated from ¹H saturation recovery experiments and ranged from 0.5 s to 5 s.

Dielectric Spectroscopy. The powder samples were loaded onto the surface of coplanar interdigitated electrode capacitors fabricated by gold metallization on fused-silica substrates (each with 50 fingers separated by $\sim 10 \mu$ m gaps). Nominal capacitor values for the empty capacitors were near 1 pF and dielectric loss tangents were at or below the level of 10–15. An Andeen–Hagerling capacitance bridge was used to measure the dielectric loss and capacitance with sinusoidal alternating voltage (1.8–5 V and 0.12–12 kHz) applied to the capacitor. The data were taken continuously with the temperature slowly changing between 7 K and room temperature. The curves were averaged over heating and cooling steps and smoothed.

Calculations. All calculations of dipole moments were carried out in the Gaussian 16, C.01 program package.² Geometry optimization was performed *in vacuo*, at the B3LYP/6-31G* level of theory with Grimme's empirical dispersion correction with Becke–Johnson damping (GD3BJ).

Starting from this geometry, single-point calculations *in vacuo* were performed using various functionals (B3LYP, CAM-B3LYP, BMK, PBE1PBE, BHandHLYP, M06 and M062X) with 6-311+G(d,p), cc-pVDZ and cc-pVTZ basis sets. Dipole moments from each of these calculations are shown in Table S1.

A TPP hexamer (supercell containing six TPP molecules) was extracted from its crystal structure.³ This nonperiodic geometry was then optimized using the GFN2-xTB method with all nitrogen and phosphorous atoms constrained by a 10 kcal mol⁻¹ \AA^{-2} harmonic potential, which allowed only small changes in their positions during the optimization (the RMSD of N and P between the crystal structure and the xTB-GFN2 optimized geometry was 0.04 \AA). The overall RMSD (excluding hydrogens) between the crystal structure and the optimized geometry was found to be 0.27 \AA , mostly due to the movement of the outer phenyls ($\sim 0.45 \text{ \AA}$), while the

inner phenyls moved much less (~0.15 Å, see Figure S3). This hexamer geometry was used as a starting point for all subsequent calculations.

In all subsequent GFN2-xTB simulations, the constraining potential on N and P was increased to 10 kcal mol⁻¹ Å⁻² to prevent the geometry from distorting further away from the solid-state structure. Preliminary optimization of **1**@TPP found two distinct minima (similar to complexes **I** and **III**). The conformational space around these was explored further by GFN2-xTB metadynamics, which were run for 20 ps for each minimum with a 1 fs timestep. The collective variable was constructed from the positions of atoms belonging to **1**. After removing duplicates using CREST (RMSD = 0.125 Å), all obtained geometries were optimized with GFN2-xTB, and finally reoptimized at the B3LYP-D3BJ/def2-SVP level of theory using Gaussian16.² The barrier for rotation of **1** while inside TPP was estimated by performing a relaxed scan in both directions with a resolution of 5° at B3LYP-D3BJ/def2-SVP, starting from **I** (Figure S1). The energy landscape for translation of **1** in the channel was obtained by relaxed scans starting from either **I** and moving outward or **III** and moving inward, in increments of 0.1 Å (Figure S2). In all DFT calculations, the positions of N and P atoms were kept fixed.

NMR shieldings were calculated for the DFT optimized structures at the same level of theory (B3LYP-D3BJ/def2-SVP). The shieldings of three *t*-Bu carbon atoms were averaged. Note that to convert the calculated shieldings (σ) into chemical shifts (δ), one has to subtract the shielding from a reference. However, chemical-shift differences between individual structures can be easily calculated, for example: $\delta(\text{III}) - \delta(\text{I}) = \sigma(\text{I}) - \sigma(\text{III})$.

Procedures. Analytical thin-layer chromatography (TLC) was performed using precoated TLC aluminum sheets (Silica gel 60 F₂₅₄). TLC spots were visualized using either UV light (254 nm) or a 5% solution of phosphomolybdic acid in ethanol, and heat (400 °C) as a developing agent. Flash chromatography was performed using silica gel (high-purity grade, the pore size of 60 Å, 70–230 mesh). Melting points are reported uncorrected. Chemical shifts in ¹H and ¹³C spectra are reported in ppm on the δ scale relative to CHCl₃ ($\delta = 7.26$ ppm for ¹H and $\delta = 77.2$ ppm for ¹³C), acetone-*d*₆ ($\delta = 2.05$ ppm for ¹H and $\delta = 29.8$ ppm for ¹³C) as internal references. For solubility reasons, the NMR spectra of **1** were recorded in CS₂ with acetone-*d*₆ as an internal standard. Structural assignments were made with additional information from gCOSY, gHSQC and gHMBC experiments. The volume/volume (v/v) ratios of solvents were used to prepare mobile phases for column chromatography.

High-resolution mass spectra (HRMS) using the matrix-assisted laser desorption/ionization (MALDI) mode were recorded on a time-of-flight (TOF) mass spectrometer.

Surface Inclusions. The surface inclusions are marked as X%**1**@TPP-*d*₁₂, where X represents the molar ratio of the molecular rotor **1**. The samples were prepared by mixing solid **1** and TPP-*d*₁₂ in defined molar ratios according to our previously published procedure.⁴

Synthesis

Molecular Rotor (1). A vacuum-dried and argon-filled round-bottom flask equipped with a magnetic stir bar was charged with C₆₀ (100 mg, 0.14 mmol, 1.0 equiv.) and THF (30 mL), and the brown suspension was sonicated under an inert atmosphere for at least 18 h at room temperature. Subsequently, **4** (64 mg, 0.20 mmol, 1.4 equiv.) followed by a freshly prepared solution of LHMDS in THF (1.0 M, 0.25 mmol, 250 μ L) was added dropwise to the greenish-brown suspension at room temperature over 30 min. The dark reaction mixture was stirred for 30 min at the same temperature and the second portion of LHMDS in THF (1.0 M, 0.25 mmol, 250 μ L) was introduced dropwise over 30 min. As the reaction progressed, the color of the reaction mixture turned to deep bluish-black. Progress of the reaction was monitored using TLC. (Sample preparation: 50 μ L of the reaction mixture was evaporated, the dark solid residue was dissolved in 1 mL of CS₂ and a small sample was used for the TLC analysis, which was developed in a 1:1 mixture of CS₂/hexane. The formation of **1** was confirmed by the appearance of a new dark brown spot with R_f = 0.70. The R_f of C₆₀ was 0.90.) The crude reaction mixture was quenched with trifluoroacetic acid (300 μ L, 4 mmol) and the volatiles were removed under reduced pressure. The dark-brown crude product was purified using repeated column chromatography on silica gel, the first of which involved the elution of a mixture of **1** and C₆₀ with pure CS₂. The remaining column chromatography purifications were performed in pure hexane, which was gradually transformed into pure CS₂. Compound **1** was finally obtained as a dark-brown solid (25 mg, 0.03 mmol, 21%).

Mp > 300 °C (dec.). ¹H NMR (400 MHz, CS₂ with acetone-*d*₆ as an internal standard): δ 0.70 (s, 9H), 6.39 (s, 1H), 6.72 (d, *J* = 8.4 Hz, 2H), 6.93 (d, *J* = 8.4 Hz, 2H). ¹³C {¹H} (100 MHz, CS₂/acetone-*d*₆): δ 31.61, 34.84, 55.46 (sp³ carbon of the C₆₀), 62.39 (CH of the C₆₀), 84.69, 92.14, 119.93, 125.91, 132.31, 135.42, 136.47, 140.67, 140.71, 141.94, 142.03, 142.22, 142.34, 142.36, 142.44, 142.89, 142.92, 143.33, 143.53, 144.84, 144.99, 145.65, 145.71, 145.82, 145.94, 146.00, 146.08, 146.52, 146.69, 146.97, 147.61, 147.87, 151.63, 151.77, 152.02. IR (KBr): 3083, 3033, 2957, 2922, 2864, 2329, 2221, 1513, 1501, 1428, 1392, 1362, 1266, 1188, 832, 573, 527 cm⁻¹. MALDI-TOF *m/z*: [M⁺] calcd. for C₇₂H₁₄⁺ 878.1096, found 878.1112. Anal. calcd. for C₇₂H₁₄: C, 98.39; H, 1.61. Found: C, 98.50; H, 1.38.

1-(tert-Butyl)-4-ethynylbenzene (4). A previously published procedure⁵ was adapted as follows: To a solution of **3** (500 mg, 2.2 mmol, 1.0 equiv.) in THF (10 mL) was added TBAF in THF (1 M, 2.6 mL, 1.2 equiv.). The reaction mixture was stirred at room temperature for 30 min. Subsequently, the reaction mixture was diluted with CH₂Cl₂ (10 mL) and washed with water (1 \times 5 mL). The organic phase was dried over MgSO₄ and the solvent was removed under reduced pressure. Column chromatography on silica gel (hexane) afforded **4** as a colorless oil (260 mg, 1.64 mmol, 76%).

¹H NMR (CDCl₃, 400 MHz): δ 1.32 (s, 9H), 3.03 (s, 1H), 7.35 (d, *J* = 8.5 Hz, 2H), 7.44 (d, *J* = 8.5 Hz, 2H). ¹³C {¹H} NMR (CDCl₃, 100 MHz): δ 31.3, 35.0, 84.0, 119.2, 125.5, 132.0, 152.2.

Calculations of the Dipole Moment of Molecular Rotor 1

All calculations were carried out in Gaussian 16, C.01 program package.² Geometry optimization was performed *in vacuo*, B3LYP/6-31G* level of theory with Grimme's empirical dispersion correction with Becke-Johnson damping (GD3BJ).

Starting from this geometry, single point calculations *in vacuo* were done using various functionals (B3LYP, CAM-B3LYP, BMK, PBE1PBE, BHandHLYP, M06 and M062X) with 6-311+G(d,p), cc-pVDZ and cc-pVTZ basis sets. Dipole moments from each of these calculations are shown in **Table S1**.

Table S1. Evaluation of the dipolar moment of molecular rotor 1.

	Dipole Moment (Debye)		
	6-311+G(d,p)	cc-pVDZ	cc-pVTZ
B3LYP	4.17	3.80	3.92
CAM-B3LYP	4.14	3.78	3.91
PBE1PBE	4.33	4.15	4.09
BMK	4.30	4.16	4.11
BHandHLYP	4.26	3.95	4.03
M06	4.00	3.98	3.79
M062X	4.24	4.10	4.08

Interpretation of NMR Spectra

The ^{13}C NMR spectrum of **1** in solution contains several characteristic resonances which can be used as NMR probes. Starting at low values of chemical shifts, the *t*-Bu group is characterized by two signals at 31.6 and 34.8 ppm. The first one belongs to three equivalent methyls and the other one represents aliphatic quaternary carbon atom. The second pair of signals at 55.5 and 62.4 ppm belongs to the fullerene unit, where the first resonance represents a quaternary carbon atom carrying an alkynyl residue and the peak at 62.4 comes from the CH group. The third pair of peaks at 84.7 and 92.1 ppm originates from triple-bond carbon atoms, with the first one being next to the phenyl ring and the second one being connected to the C_{60} unit. The signals of all aromatic carbon atoms appear between 120.0 and 152.0 ppm (Figures 1 and 4A).

The solid-state ^{13}C cross-polarization magic-angle spinning (CP MAS) NMR spectrum of neat **1** resembles its solution spectrum except for the aromatic region, where all carbon resonances have collapsed into seven broad peaks (Figure 3B). The CP MAS spectra of both inclusions (5%**1**@TPP- d_{12} and 10%**1**@TPP- d_{12}) are dominated by three peaks in the aromatic region (Figures 4C and 4D), which are caused by the hexagonal TPP- d_{12} (144.4, 124.1 and 122.5 ppm). The appearance of these signals indicates the successful formation of the inclusion. The protonated guest molecules that are in close proximity to the interior of TPP channels successfully mediate the through-space transfer of polarization from the guest molecules to the carbon atoms of the perdeuterated matrix. The three equivalent methyl carbon atoms of the *t*-Bu group represent probably the most diagnostic peak characterizing the guest molecule **1** in both inclusions (Figures 4C and 4D). Surprisingly enough, this peak (30.6 ppm) has a distinct shoulder (31.4 ppm) in 5%**1**@TPP- d_{12} (Figure 3C). Both of these peaks are upfield-shifted in comparison with the solution spectrum (31.6 ppm). The remaining peaks representing **1** are either invisible due to their low intensity or overlap with the TPP signals. Upfield shifts are characteristic of inclusion complexes because the individual catechol-based aromatic rings forming TPP channels (Chart 1) effectively shield the carbon nuclei of included molecules.

The ^{13}C CP MAS NMR spectrum of 10%**1**@TPP- d_{12} is richer in the 30–100 pm region than that of 5%**1**@TPP- d_{12} . There are two peaks at 30.7 and 31.9 ppm in a roughly 1:1 ratio due to the carbons of two inequivalent *t*-Bu groups, with the first one upfield shifted toward 31.6 ppm in solution and the second one shifted slightly downfield. One of the two inequivalent *t*-Bu quaternary carbon atoms at 34.6 ppm is also slightly upfield shifted in comparison with 34.8 ppm in solution. The second one most likely overlaps with the signals belonging to the methyl groups. The two resonances at 55.1 and 62.0 ppm, representing the C_{60} unit, are slightly upfield shifted when compared to the solution spectrum as well. This can be explained by the specific shielding of these two nuclei by the TPP surface. The peak at 84.1 ppm, which represents the triple bond carbon atom next to the phenyl ring, is upfield shifted, indicating that this part of the molecule is still immersed in the TPP matrix. The second triple bond carbon atom at 92.6 ppm, which is next to the C_{60} unit, is downfield shifted, which implies that this part of the molecule is above the surface. The relatively low signal-to-noise ratio of these last four peaks does not make it possible to determine whether they have shoulders or are doubled. The resonances of aromatic carbon atoms coming mostly from the fullerene unit overlap with the intense signals of the TPP matrix.

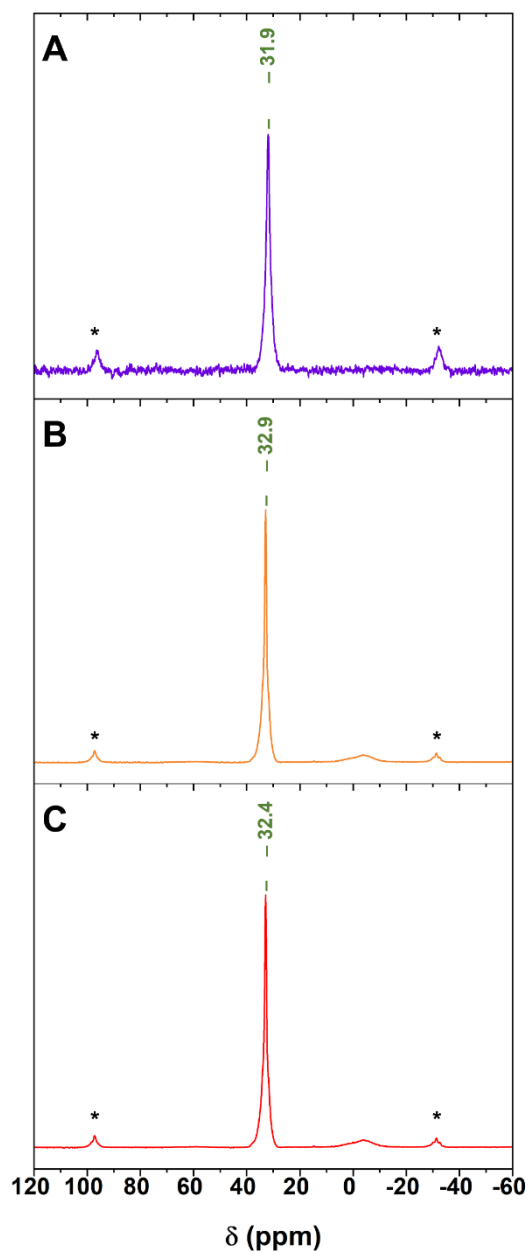


Figure S1. ^{31}P CP MAS NMR: 5% **1**@TPP- d_{12} (A), 10% **1**@TPP- d_{12} (B), and 10% **1**@TPP- d_{12} diluted with an excess of fresh hexagonal TPP- d_{12} (C). Asterisks indicate spinning sidebands.

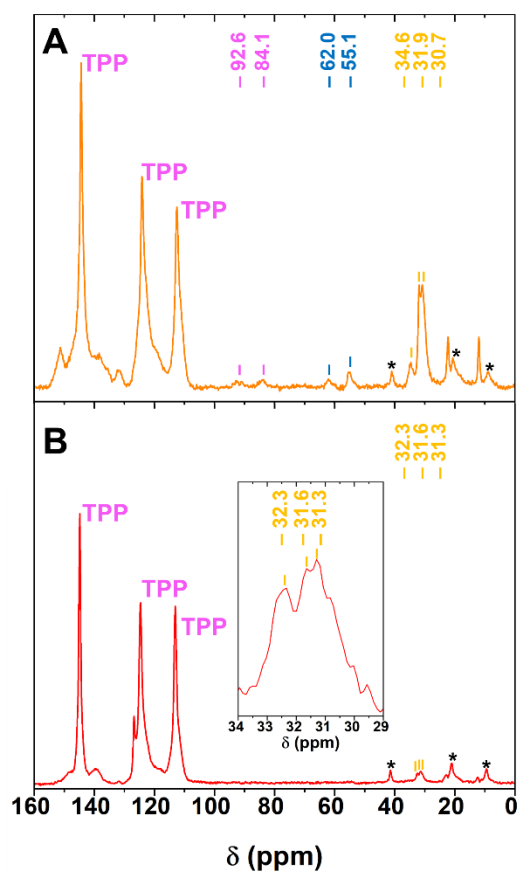


Figure S2. ^{13}C CP MAS NMR: 10% **1**@TPP- d_{12} (A), and 10% **1**@TPP- d_{12} diluted with an excess of fresh hexagonal TPP- d_{12} (B). Asterisks indicate spinning sidebands.

Computational Investigation of 1@TPP

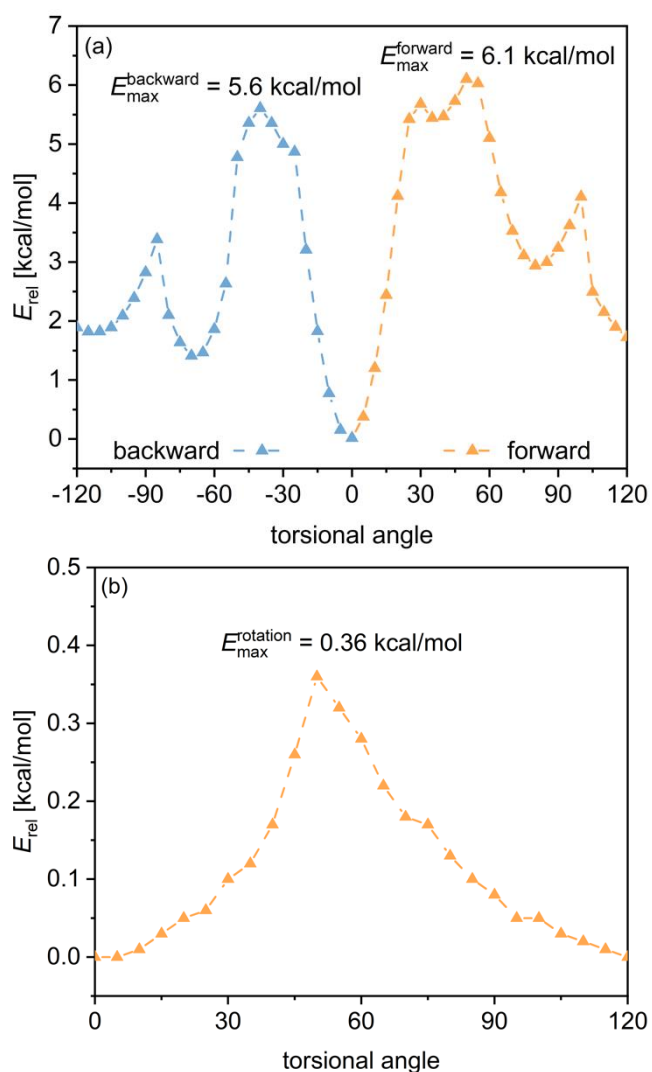


Figure S3. Energy profile for rotation of conformer **I** (a) and conformer **III** (b) in of **1@TPP**, obtained by relaxed scans in 5° increments at B3LYP-D3BJ/def2-SVP. In case of **III**, forward and backward movement converge to nearly identical minima.

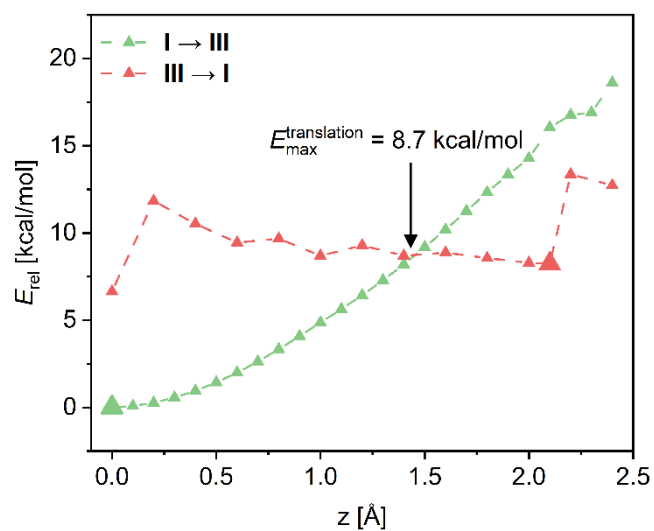


Figure S4. Energy profile for translation interconverting **I** and **III**, obtained at B3LYP-D3BJ/def2-SVP.

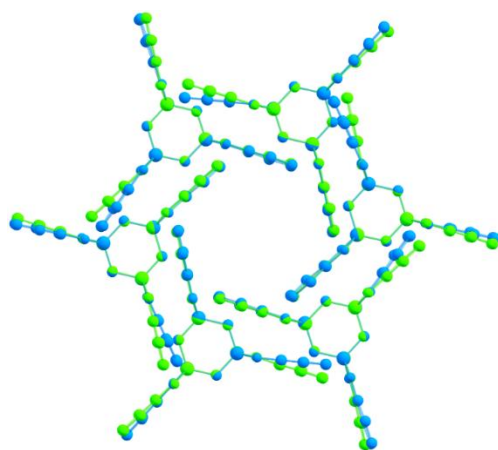
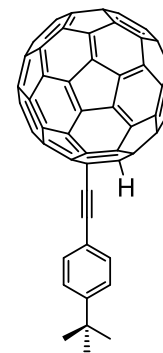
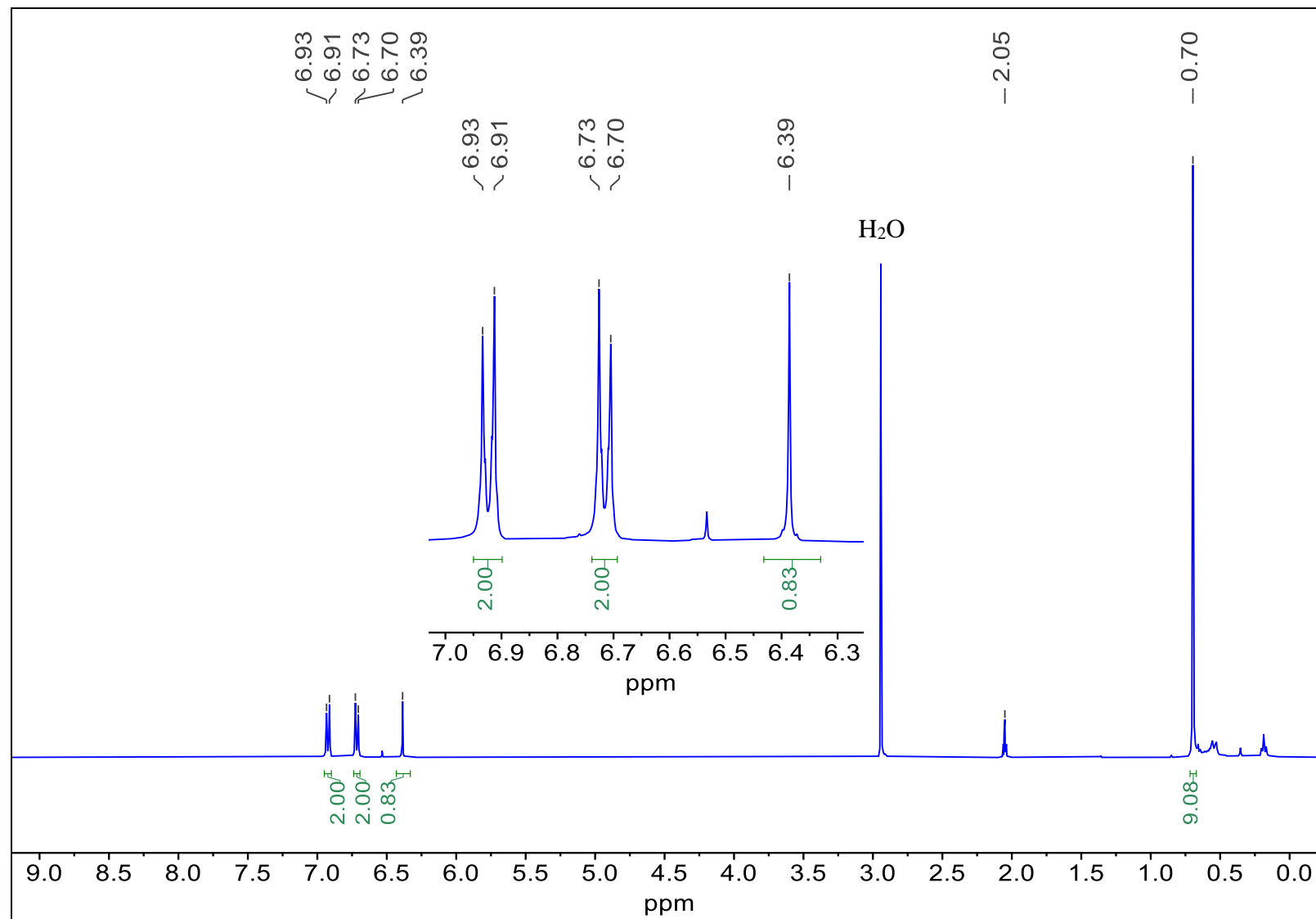
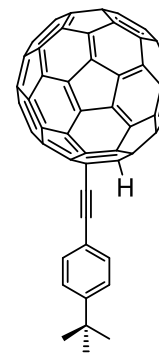
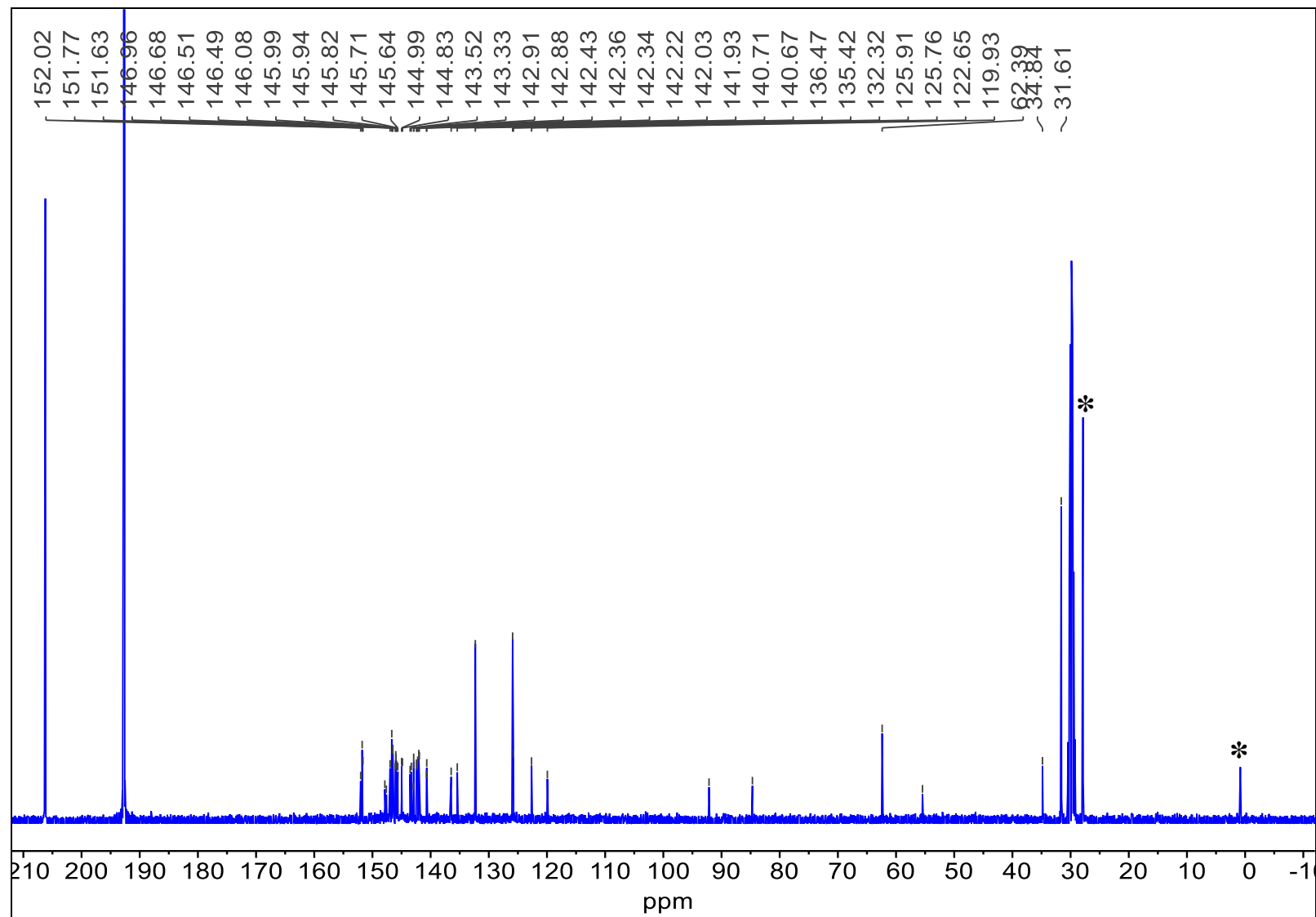


Figure S5. An overlay between the crystal structure of TPP (green) and the optimized hexamer geometry (blue).

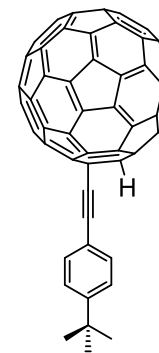
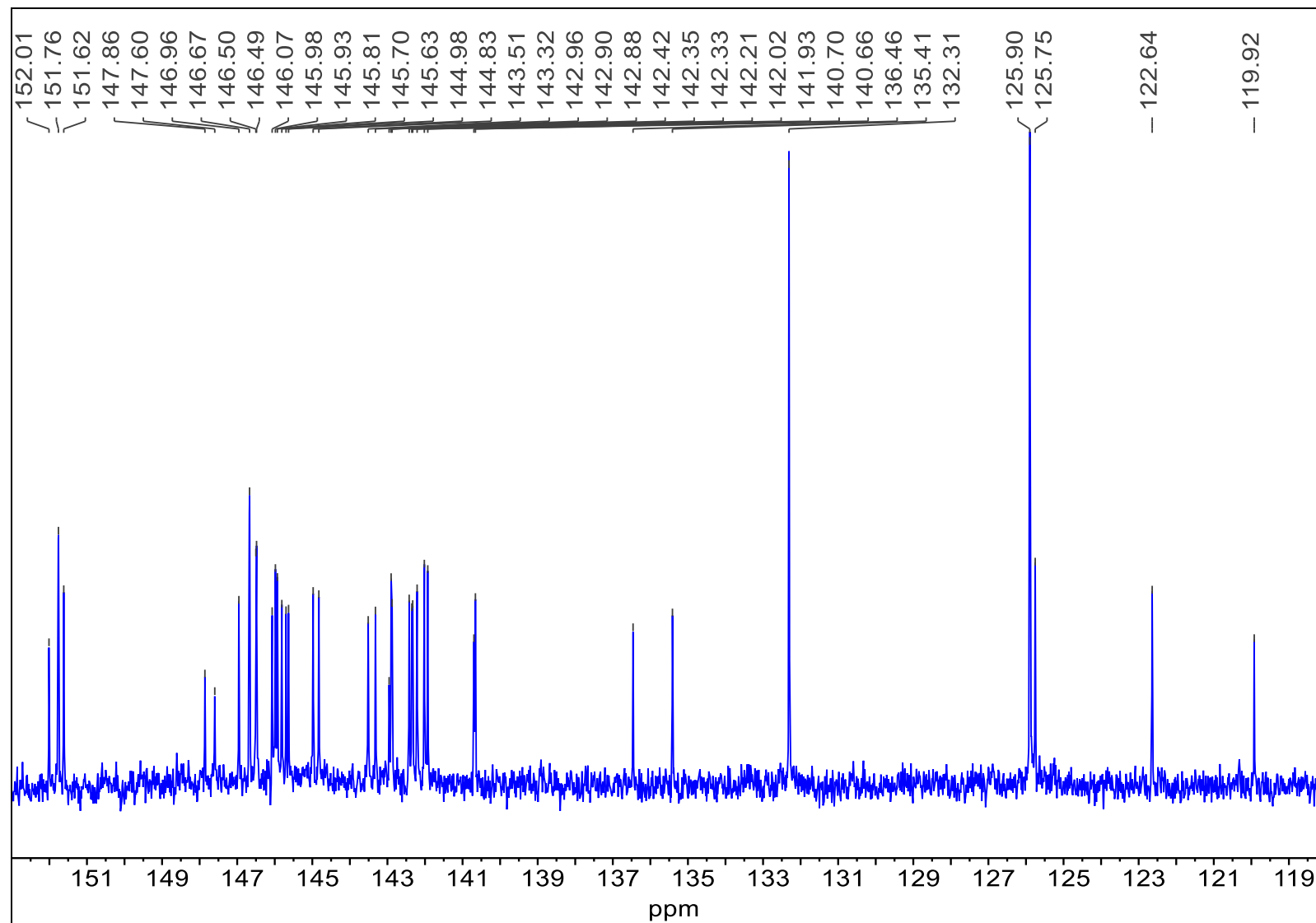
^1H NMR (400 MHz, CS_2 with acetone- d_6 as an internal standard): Molecular Rotor (**1**)



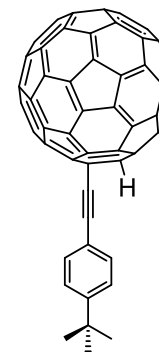
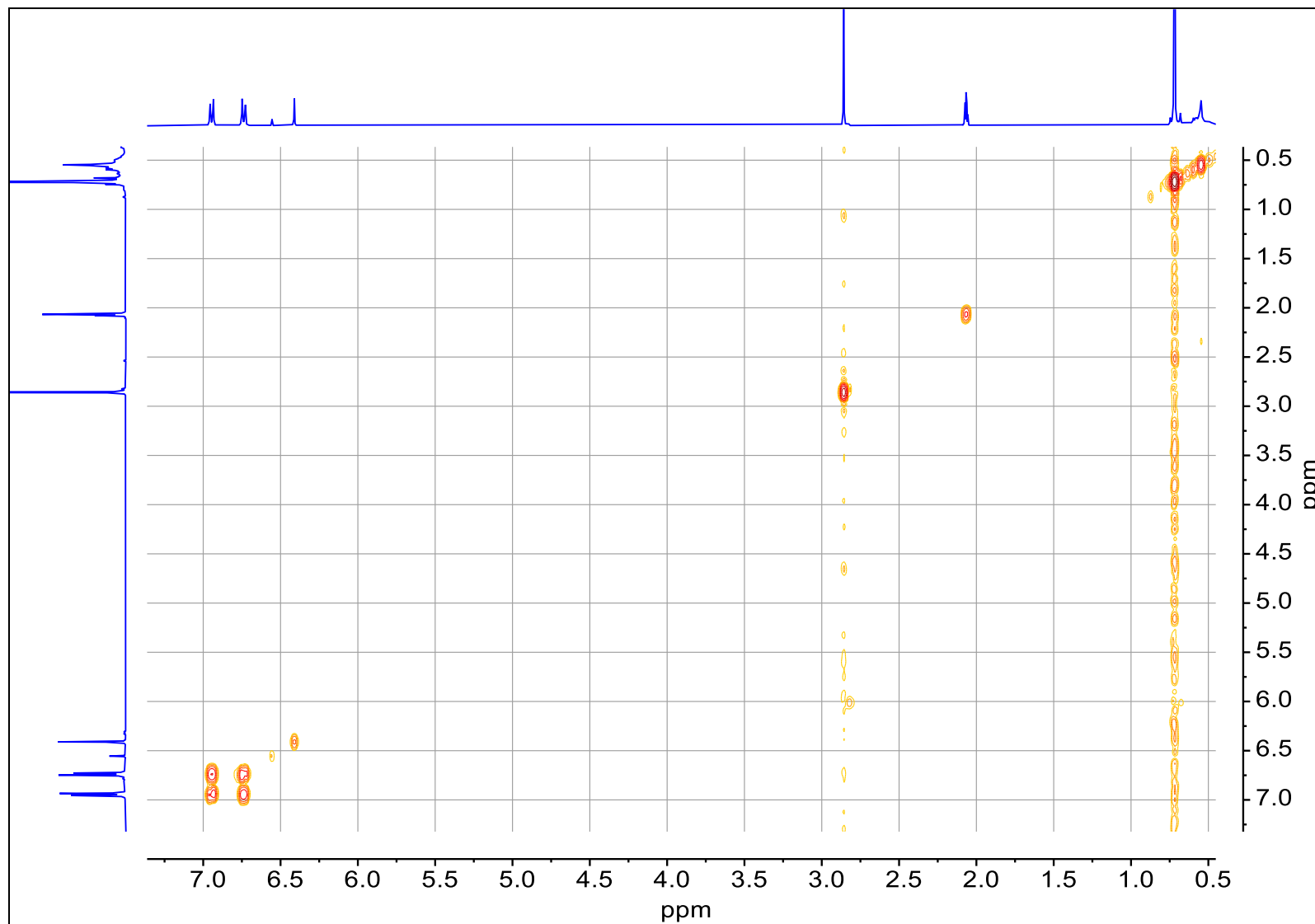
^{13}C $\{^1\text{H}\}$ NMR (400 MHz, $\text{CS}_2/\text{acetone-}d_6$): Molecular Rotor (**1**)



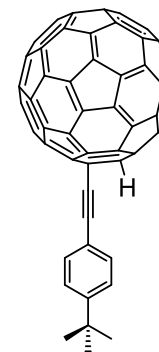
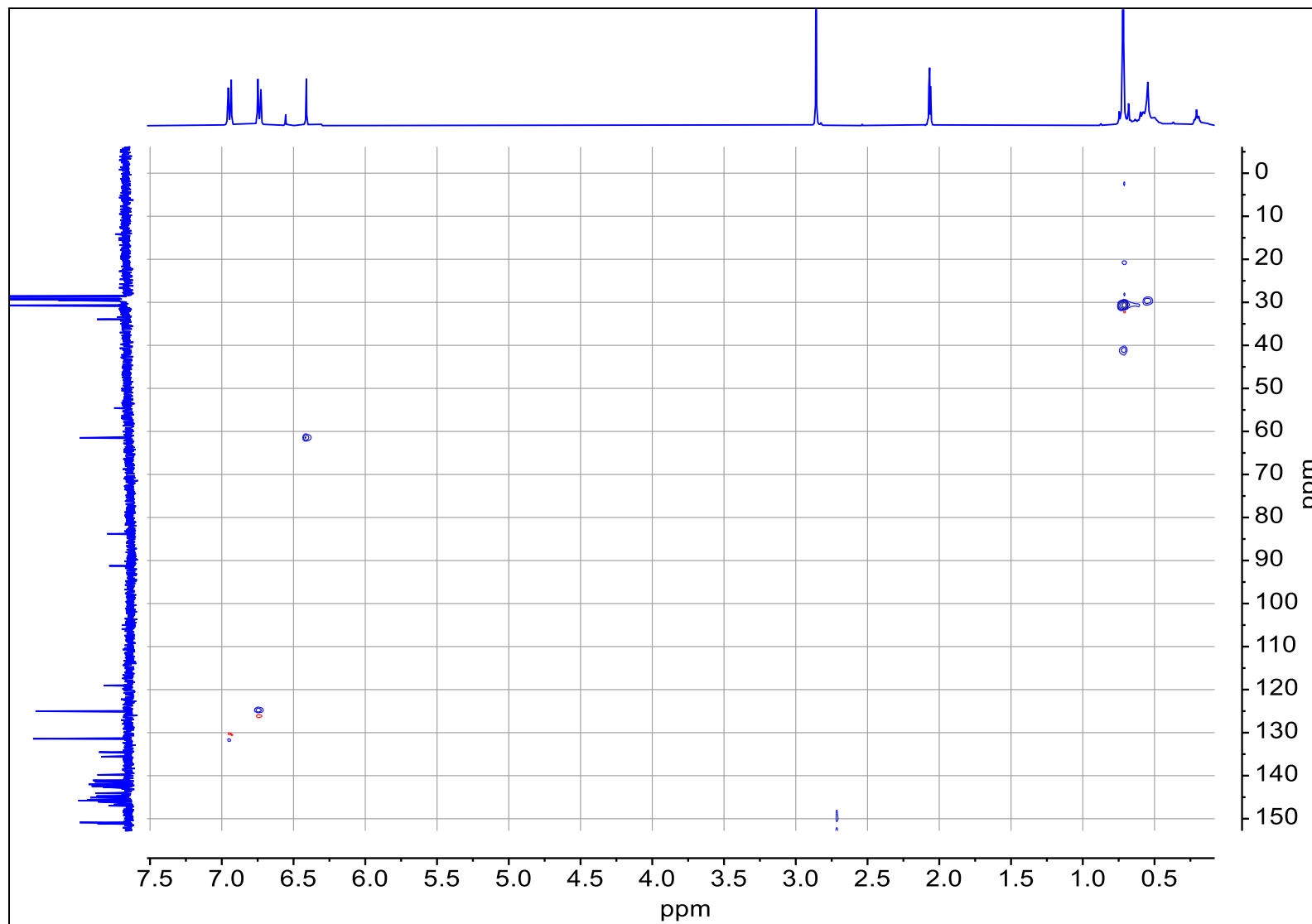
^{13}C $\{^1\text{H}\}$ NMR (100 MHz, $\text{CS}_2/\text{acetone-}d_6$) (zoom): Molecular Rotor (**1**)



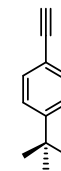
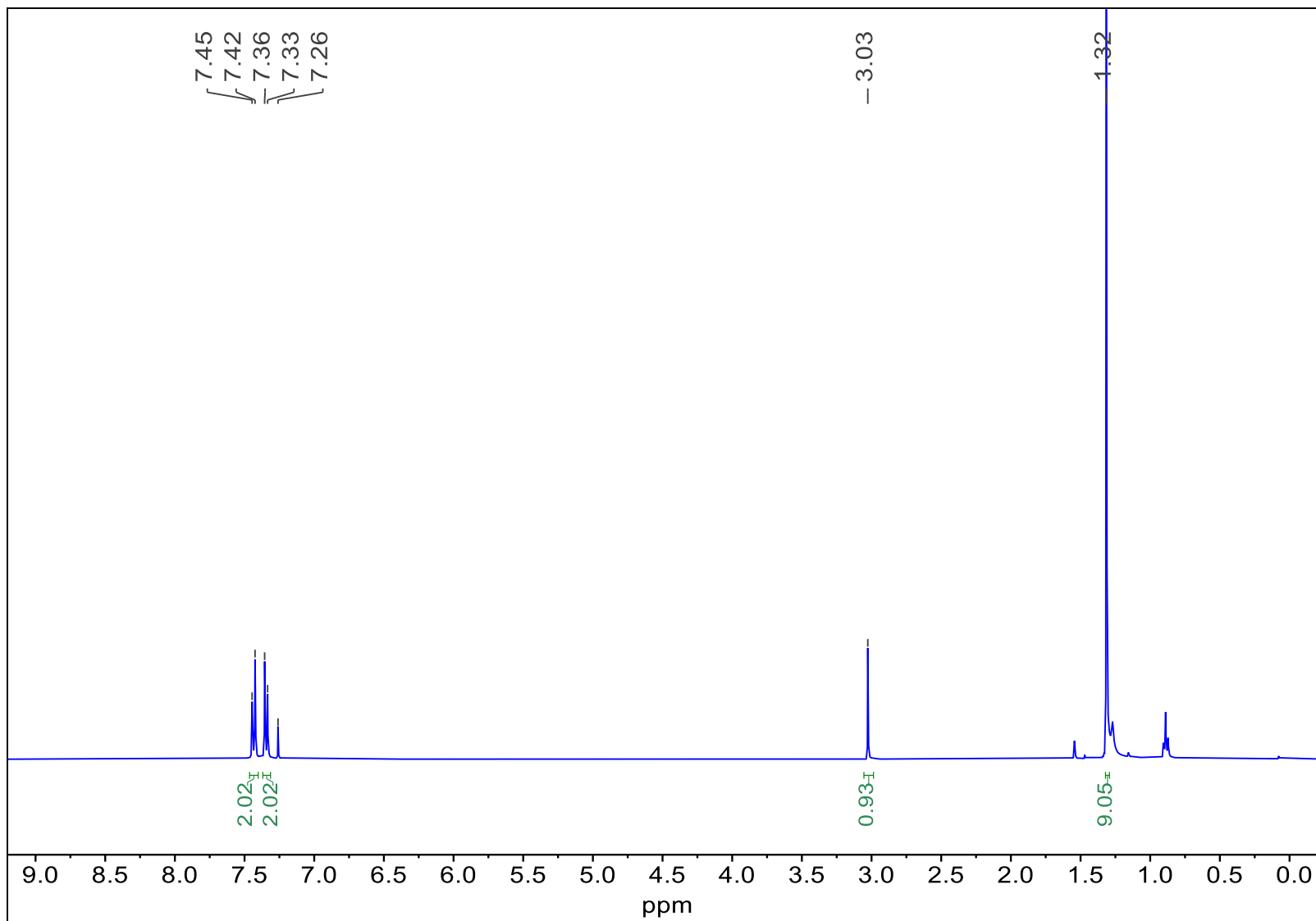
$^1\text{H} - ^1\text{H}$ COSY (400 MHz, $\text{CS}_2/\text{acetone-}d_6$): Molecular Rotor (**1**)



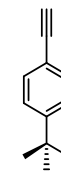
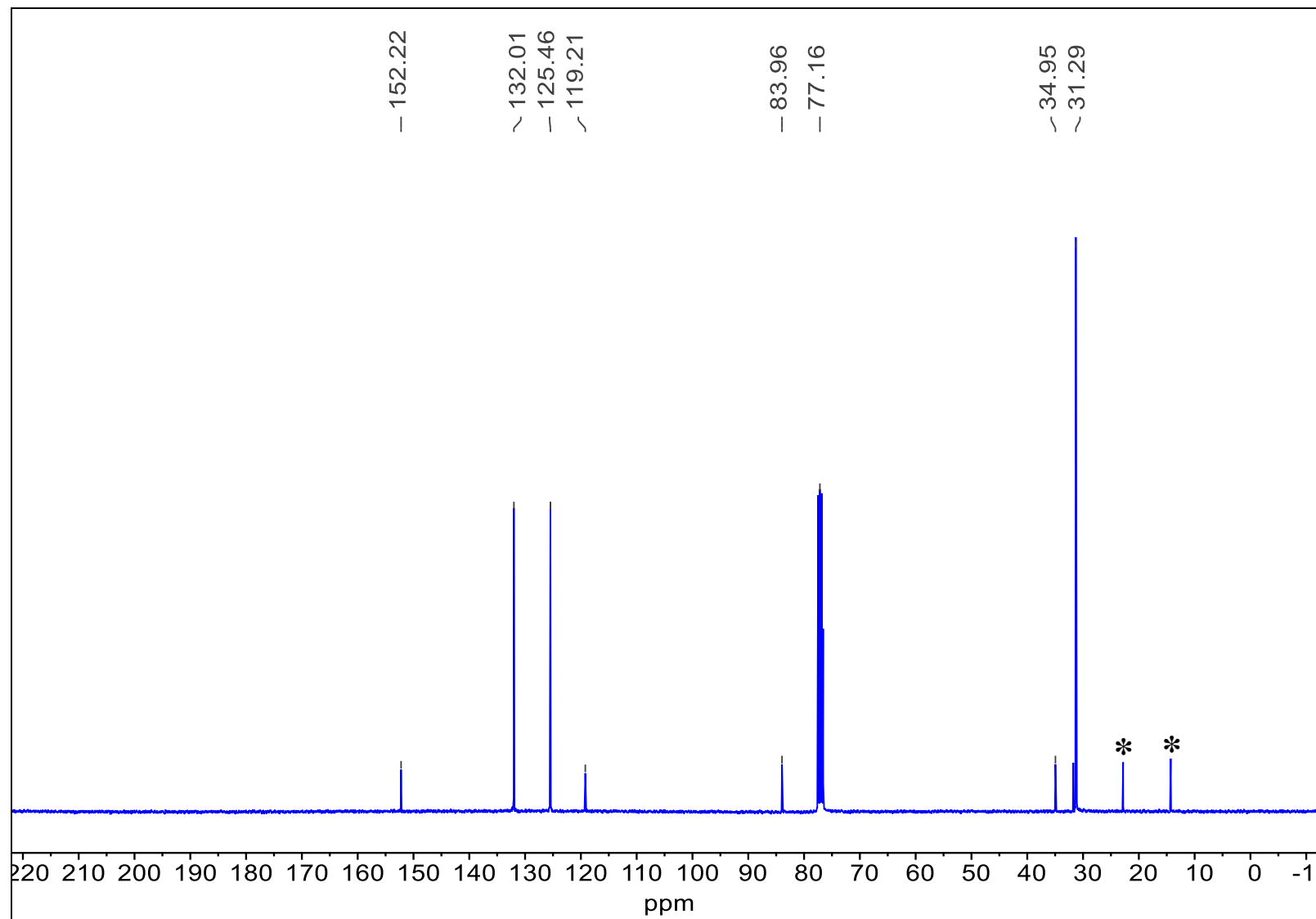
HMBC (400 MHz, CS₂/acetone-*d*₆): Molecular Rotor (**1**)



¹H NMR (400 MHz, CDCl₃): 1-(*tert*-Butyl)-4-ethynylbenzene (**4**)



^{13}C $\{^1\text{H}\}$ NMR (100 MHz, CDCl_3): 1-(*tert*-Butyl)-4-ethynylbenzene (**4**)



References

1. Sato, A. H.; Mihara, S.; Iwasawa, T. "One-Step Synthesis of (1-Iodovinyl) Arenes from Trimethylsilyl Ethynylarene through Iodotrimethylsilane-Mediated Hydroiodation." *Tetrahedron Lett.* **2012**, *53*, 3585–3589.
2. Gaussian 16, Revision C.01, M. J. Frisch, G. W. Trucks, H. B. Schlegel, G. E. Scuseria, M. A. Robb, J. R. Cheeseman, G. Scalmani, V. Barone, G. A. Petersson, H. Nakatsuji, X. Li, M. Caricato, A. V. Marenich, J. Bloino, B. G. Janesko, R. Gomperts, B. Mennucci, H. P. Hratchian, J. V. Ortiz, A. F. Izmaylov, J. L. Sonnenberg, D. Williams-Young, F. Ding, F. Lipparini, F. Egidi, J. Goings, B. Peng, A. Petrone, T. Henderson, D. Ranasinghe, V. G. Zakrzewski, J. Gao, N. Rega, G. Zheng, W. Liang, M. Hada, M. Ehara, K. Toyota, R. Fukuda, J. Hasegawa, M. Ishida, T. Nakajima, Y. Honda, O. Kitao, H. Nakai, T. Vreven, K. Throssell, J. A. Montgomery, Jr., J. E. Peralta, F. Ogliaro, M. J. Bearpark, J. J. Heyd, E. N. Brothers, K. N. Kudin, V. N. Staroverov, T. A. Keith, R. Kobayashi, J. Normand, K. Raghavachari, A. P. Rendell, J. C. Burant, S. S. Iyengar, J. Tomasi, M. Cossi, J. M. Millam, M. Klene, C. Adamo, R. Cammi, J. W. Ochterski, R. L. Martin, K. Morokuma, O. Farkas, J. B. Foresman, and D. J. Fox, Gaussian, Inc., Wallingford CT, 2019.
3. Comotti, A.; Bracco, S.; Ferretti, L.; Mauri, M.; Simonutti, R.; Sozzani, P. "A Single-Crystal Imprints Macroscopic Orientation on Xenon Atoms." *Chem. Commun.* **2007**, 350-352.
4. Kaleta, J.; Chen, J.; Bastien, G.; Dračinský, M.; Mašát, M.; Rogers, C. T.; Feringa, B. L.; Michl, J. "Surface Inclusion of Unidirectional Molecular Motors in Hexagonal Tris(*o*-phenylenedioxy)cyclotriphosphazene TPP." *J. Am. Chem. Soc.* **2017**, *139*, 10486–10498.
5. Thiel, N. O.; Kemper, S.; Teichert, J. F. "Copper(I)-catalyzed Stereoselective Hydrogenation of 1,3-Diynes and Enynes." *Tetrahedron.* **2017**, *73*, 5023–5028.